Sliding Mode Wheel Slip Control for Regenerative Braking of an All Wheel Drive Electric Vehicle *†

Abhigyan Majumdar
Graduate Student
Department of Mechanical & Aerospace Engineering
University of California
Davis, California 95616
Email: abmajumdar@ucdavis.edu

Shima Nazari
Assistant Professor
Department of Mechanical & Aerospace Engineering
University of California
Davis, California 95616
Email: snazari@ucdavis.edu

Regenerative braking is one of the main advantages of electric propulsion systems. In such systems, the vehicle brake controller has to prioritize safety while maximizing the recovered energy at all times. This paper proposes a two-step hierarchical brake controller for a dual-motor all-wheel-drive electric vehicle. In the first step, a novel sliding mode controller (SMC) generates the total braking torque on each axle to independently control the slip on the front and rear wheels. In the second step, the torque split controller assigns motor and friction brake torques to maximize the recovered energy. By incorporating the effects of changing vehicle speed, the proposed SMC controller accounts for the non-linearities in vehicle dynamics and tire model, and considers the weight transfer due to vehicle deceleration, while being robust to disturbances. Using simulations, we show that while the traditional SMC formulation is not effective during emergency braking scenarios, the proposed formulation successfully generates control commands to bring the vehicle to a stop position at a minimum distance. Furthermore, our controller can maintain both wheels in the stable slip region, even when starting from a locked position. The performance of the proposed controller is evaluated for an emergency braking scenario and on an aggressive segment of the US06 cycle.

*Paper presented at the 2023 Modeling, Estimation, and Control Conference (MECC 2023), Lake Tahoe, NV, Oct. 2-5. Paper No. MECC2023-141.

†This work was partially funded by support from the U.S. Department of Energy EcoCAR EV Challenge.

1 Introduction

As the Electric Vehicle (EV) market keeps growing and maturing, it is increasingly important to maximize the safety, reliability, and fuel economy of these cars for higher competitiveness compared to traditional cars. One particular challenge is that of wheel slip and traction control. Especially for all-wheel-drive (AWD) EVs with multiple sources of propulsion and braking, it is critical that the onboard controllers deploy the right combination of these available actuators to maximize safety, dynamic performance, and energy efficiency. In the case of braking control, for example, the braking torque distribution greatly influences both the vehicle fuel economy and safety. Most fuel economy benefits of electrification are undermined if the vehicle wastes energy in friction brakes rather than recuperating through the electric motors. On the other hand, effective braking is critical for ensuring safe vehicle handling in different driving conditions, such that numerous researchers have investigated the problem over the years.

Researchers have preferred model-based controllers over rule-based ones because of the continuous control action that ensures smoother system response and longer actuator life, as noted by the authors in [1]. However, model-based controller design has challenges associated with parameter identification and developing simple yet accurate system models that account for critical system dynamics. Sliding mode controllers (SMC) are advantageous in this regard due to their inherent robustness to external disturbances, model parameter uncertainties, and how they retain the complex non-linearities and dynamics in the system [2], [3], [4]. Many studies, such as one in [5], have relied on simplified and linearized models for controller development and anal-

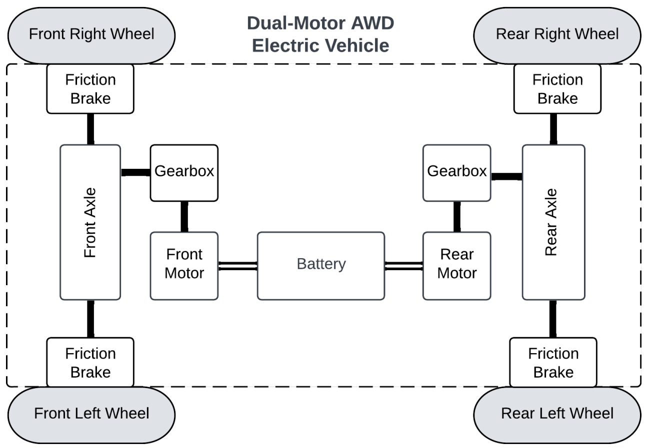

Fig. 1. Schematic diagram of dual-motor AWD electric vehicle

ysis, in which the interdependencies of the system dynamics vanish in the linearization process. Therefore, non-linear control techniques such as Sliding Mode Control (SMC) were perceived as more suitable methods in [6].

SMC has been used in different control architectures for traction and braking control. In [1], the authors addressed the issue of sluggish brake actuators and chattering in SMCs by considering frequency shaping of the sliding surface to introduce tolerance to delays in physical sensors and actuators. The authors of [2] developed a second-order SMC coupled to a first-order sliding mode observer for wheel slip control. Although the combined observer and controller were able to handle disturbances and parameter variations, the control torque appeared to have low amplitude high-frequency oscillations when simulated in icy road conditions without input disturbances or parameter variation. In [7], the authors developed a first-order SMC considering the uncertainty in longitudinal speed and acceleration. Their method was able to handle white noise in lateral tire force feedback. In [8], the authors used an integral switching surface for their SMC formulation based on a longitudinal vehicle model considering separate sprung and unsprung masses. The developed controller was found to perform better than fuzzy logic, neural network, and self-learning fuzzy-SMC controllers from previous literature. Researchers in [3] developed an SMC controller using an exponential law for a smoother target following. The controller was found to be robust to errors in motor torque and adhesion coefficient. However, tests on a real vehicle showed chattering in slip ratio, with oscillations and overshoot. In [4], the authors combined a low-pass filter with the SMC control law to reduce the chattering phenomenon. The authors of [9] developed a combining sliding mode controller that fused the advantages of wheel slip and wheel deceleration control for better stability and quicker response. However, their results showed high-frequency oscillations in the wheel slip and wheel deceleration towards the end of the simulations. These prior studies highlight the need for improved stability, smoothness, and responsiveness in the SMC controller response.

In this work, we developed a controller to retain high responsiveness throughout the vehicle speed range, while providing smooth, chatter-free actuation commands. We incorporate the vehicle speed in the controller formulation, improving responsiveness throughout the vehicle speed range. AWD EV architectures, such as the one shown in Fig. (1) have one motor on each axle and therefore have intense acceleration and braking capabilities, such that the vertical tire loads change significantly during such maneuvers. For this study, we used a coupled non-linear model to describe our system, that accounts for longitudinal weight transfer. Furthermore, the Pacejka tire model, which captures the non-linear nature of the tire-road interaction, is used to model the longitudinal tractive force at the wheels. A novel sliding mode control law is proposed in Section 2.2 to individually regulate the longitudinal slip ratio for each axle. The proof for controller stability is provided in Section 3. The performance of the developed controller is shown for the emergency braking scenario, an intense braking maneuver from the US06 cycle, and for unstable initial conditions in Section 4. The developed controller can stabilize the system and track changing references while rejecting external disturbance in the form of uncertainty in wheel slip feedback.

2 Methodology

Figure (1) shows a schematic of the dual-motor AWD electric vehicle studied here, which is similar to the 2023 Cadillac LYRIQ from General Motors. The high-voltage battery powers both the front and rear motors, and each motor is connected to the wheels through a gearbox and an open differential. In such systems, different actuators can be used for braking, namely, the front and rear motors, and the friction brakes. The braking torque control and the distribution between these actuators highly influence both the vehicle energy consumption and safety. In this section, we first present a model for the system, and then we discuss the proposed non-linear sliding mode controller.

2.1 Plant Model

In this work, the longitudinal motion of the vehicle is investigated, and thus we do not make any distinction between the left and the right wheels. The modeled states for the 2-axle vehicle are the vehicle speed, and front and rear wheel speeds. The vehicle acceleration is computed from the net external forces on the vehicle body, given as

$$\dot{V} = \frac{1}{M_v}\left(F_{x,f} + F_{x,r} - \frac{1}{2}\rho C_d A V^2\right) \tag{1}$$

where $F_{x,f}$ and $F_{x,r}$ are the longitudinal tractive forces on the front and rear axles respectively, and the last term computes the aerodynamic drag force based on the air density ρ, the drag coefficient C_d, and the frontal area A. The rotational acceleration of each wheel, front, and rear, is computed as

$$\dot{\omega}_i = \frac{1}{J_w}\left(\tau_{m,i} g_i - \tau_{b,i} - r_w F_{x,i} - \tau_{roll,i} - b_w \omega_i\right) \quad (2)$$

where $\tau_{m,i}$ is the motor torque, $\tau_{b,i}$ is the friction brake torque, g_i is the gear ratio between the corresponding electric motor and wheels, and $\tau_{roll,i}$ is the rolling resistance torque on each axle, denoted by $i = f, r$, and r_w is the loaded wheel radius. J_w is the rotational inertia of each axle, and b_w is the damping coefficient for the axles.
We consider the weight transfer due to vehicle acceleration and deceleration, thus the front and rear vertical axle loads are defined as

$$F_{z,f} = \frac{M_v}{l_f + l_r}\left(g l_r - \dot{V} h_c\right) \quad (3)$$

$$F_{z,r} = \frac{M_v}{l_f + l_r}\left(g l_r + \dot{V} h_c\right) \quad (4)$$

where, g is the gravitational acceleration, l_f and l_r are the distances of the center of gravity from the front and the rear axles respectively, and h_c is the vertical height of the center of gravity of the vehicle from the ground. The longitudinal tractive force on each axle, $F_{x,i}$, is computed using the Pacejka-Sharp magic formula tire model as

$$F_{x,i} = \mu_{eqv,i} F_{z,i} \quad (5)$$

where μ_{eqv} is the equivalent ground adhesion coefficient, given by the magic formula

$$\mu_{eqv,i} = \mu_{scale} D \sin(C \tan^{-1}(B\lambda_i - E(B\lambda_i - \tan^{-1}(B\lambda_i)))) \quad (6)$$

where, μ_{scale} is the friction scaling factor, and B, C, D, and E are the longitudinal stiffness, shape, peak, and curvature factors, all assumed to be constant. The friction scaling factor allows us to model the tire-road interaction for different road conditions, like dry asphalt, wet asphalt, snow, ice, etc.

The longitudinal wheel slip, λ_i is defined as

$$\lambda_i = \frac{\omega_i r_w - V}{\max(|\omega_i r_w|, |V|)} \quad (7)$$

This formulation ensures all driving scenarios, i.e., acceleration, deceleration, and constant velocity driving, are accounted for. During braking, which is the focus of this effort, $\omega_i r_w < V$, meaning that the longitudinal wheel slip will be negative during braking. For the rolling resistance torque, we use a tire-pressure, vertical axle load, and velocity-dependent formulation, as follows

$$\tau_{roll,i} = F_{z,i}^{\alpha} P_{tire,i}^{\beta}\left(a + b|V| + cV^2\right)\tanh(4V) r_w \quad (8)$$

where, α is the tire load exponent, β is the tire pressure exponent, a is the velocity independent term, b is the linear velocity dependent coefficient, and c is the quadratic velocity coefficient.

The battery current is computed from the net electrical power consumed or generated by the electric motors. It must be noted that during power consumption, the mechanical motor torque, $\tau_{m,i}$ is positive, making the battery current positive, and vice versa. Thus, the battery current is given as-

$$i_{batt} = \begin{cases} \frac{1}{V_b}\left(\frac{\tau_{m,f}\omega_{m,f}}{\eta_{m,f}} + \frac{\tau_{m,r}\omega_{m,r}}{\eta_{m,r}}\right) & \tau_{m,i} > 0 \\ \frac{1}{V_b}\left(\eta_{m,f}\tau_{m,f}\omega_{m,f} + \eta_{m,r}\tau_{m,r}\omega_{m,r}\right) & \tau_{m,i} \leq 0 \end{cases} \quad (9)$$

where, V_b is the terminal voltage of the battery, given by-

$$V_b = n_s\left(OCV(\zeta) - R_{int}(\zeta)\frac{i_{batt}}{n_p}\right) \quad (10)$$

where, n_s is the number of modules in series, $OCV(\zeta)$ and $R_{int}(\zeta)$ are the open circuit voltage and DC internal resistance of each cell, expressed as a function of the state of charge of the battery, ζ, and n_p is the number of cells in parallel in each module. The rate of change of the state of charge of the cells, assumed the same for all cells, is given as

$$\dot{\zeta} = \frac{-i_{batt}}{n_p Q_n} \quad (11)$$

where Q_n is the nominal charge capacity of the cells.

Before we begin with controller synthesis, we need to express all state derivatives in the proper explicit form. The state derivative for vehicle speed, given by (1), is implicit since the vertical axle loads, $F_{x,i}$, depend on the vehicle acceleration. This is converted into an explicit form using algebraic manipulations and the definitions in (3) - (8), as follows

$$\dot{V} = f_1(V, \omega_f, \omega_r) = \frac{l_f \mu_{eqv,r} + l_r \mu_{eqv,f} - 0.5 l_0 \rho C_d A V^2}{l_0 + h_c(\mu_{eqv,f} - \mu_{eqv,r})} \quad (12)$$

where, $l_0 = l_f + l_r$ is the wheelbase of the vehicle. The vehicle model defined by Eq. (1) - (10), is used for developing the non-linear controller described in Section 2.2. All model parameters were taken from that of a Model Year 2023 Cadillac LYRIQ, provided by General Motors, except for the front motor specifications, which were considered the same as the rear motor for this study.

2.2 Sliding Mode Controller

SMC is a non-linear control technique that can account for parameter and measurement uncertainties while providing good target following and stability. Fig. (2) shows the hierarchical control structure proposed in this work. In the first step, we calculate the reference slip ratio, according to Eq.s (13) and (14). The SMC controller then computes the net braking torques required at the front and rear axles given by Eq. (20). These values are then split into motor and friction brake torques by the torque split controller governed by Eq.s (23) and (24). The final control input to the plant model is a vector of 4 control signals consisting of the front and rear motor and friction brake commands. It must be noted that the PI driver block design and tuning have not been considered in this study.

The reference vehicle deceleration is computed by linearly scaling the brake pedal position, $u_b(t)$, to the combined maximum available deceleration force from the aerodynamic drag and the maximum possible braking force as follows:

$$\dot{V}_{ref} = u_b(t)\left(g\mu_{eqv,max} + \frac{\rho C_d A V^2}{2M_v}\right) \tag{13}$$

We target equal slip on the front and rear wheels and thus the reference slip, $\lambda_{ref,i}$, is computed as

$$\mu_{eqv}(\lambda_{ref,i}) = \frac{M_v\dot{V}_{ref} + 0.5\rho C_d A V^2}{M_v g} \tag{14}$$

For a slip ratio higher than the optimum value, the system is unstable. Thus, to provide bandwidth for disturbance rejection, the reference slip ratio is defined as

$$\lambda_{ref,i} = max\,(0.9 * \lambda_{opt}, \lambda_{ref,i}) \tag{15}$$

The sliding surface is defined as the error between the reference and actual slip as follows

$$S_i = \lambda_{ref,i} - \lambda_i \tag{16}$$

Our proposed sliding mode control law is defined by the time derivative of the sliding surface given as

$$\dot{S}_i = -\frac{\eta}{V} \times \text{sat}\left(\frac{S_i}{\phi_S}\right) \tag{17}$$

where

$$\text{sat}\left(\frac{S_i}{\phi_S}\right) = \begin{cases} -1, & \text{for } S_i \leq -\phi_S \\ \frac{S_i}{\phi_S}, & \text{for } -\phi_S < S_i < \phi_S \\ 1 & \text{for } S_i \geq \phi_S \end{cases}$$

in which η is a tuning parameter that controls the disturbance rejection capability of the controller, and ϕ_S is the boundary layer width that controls the extent of the region in which the sliding surface switches. In this novel formulation, the presence of the vehicle speed in the denominator ensures that the system approaches the sliding surfaces faster for lower speeds. This is unlike the traditional SMC formulation as

$$\dot{S}_{0,i} = -\eta \times \text{sat}\left(\frac{S_i}{\phi_S}\right) \tag{18}$$

Our choice of siding surface derivative was motivated by the linear analysis of a simplified longitudinal vehicle model presented in [5]. Their work showed that the linear system poles move further into the right half-plane for lower vehicle speeds, and therefore, we determined the system should reach the sliding surface quicker at lower speeds. This new formulation also improved the reference tracking ability of the controller, which is presented in Section 4. Differentiating (7) for braking scenarios, and substituting into (17), we get

$$\frac{\eta}{V} \times \text{sat}\left(\frac{S_i}{\phi_S}\right) = \dot{\lambda}_{ref,i} - \frac{r_w}{V}\left(\dot{\omega}_i - \frac{\dot{V}\omega_i}{V}\right) \tag{19}$$

Using (2), and (12), and rearranging, we get the combined net control torque input as

$$\tau_{n,i} = \tau_{m,i}g_i - \tau_{b,i} = r_w F_{x,i} + b_w\omega_i + \tau_{roll,i} + \frac{J_w}{V} f_1(V, \omega_f, \omega_r) + \frac{J_w}{r_w}\left(\dot{\lambda}_{ref,i} + \eta \times \right. \tag{20}$$

We break down the control input into two distinct parts, corresponding to the state-dependent-term and the sliding-surface-dependent-term, respectively, given as

$$u_{SMC,x}(t) = r_w F_{x,i} + b_w\omega_i + \tau_{roll,i} + \frac{J_w}{V} f_1(V, \omega_f, \omega_r) \tag{21}$$

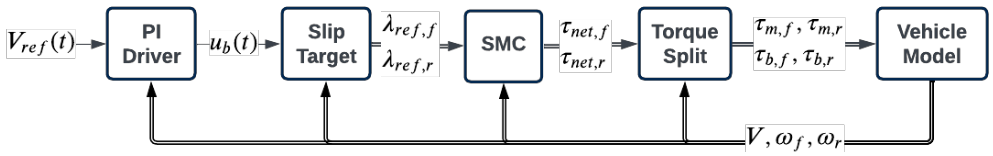

Fig. 2. Schematic diagram for the proposed closed-loop system

$$u_{SMC,S}(t) = \frac{J_w}{r_w}\left(\dot{\lambda}_{ref,i} + \eta \times \text{sat}\left(\frac{S}{\phi_S}\right)\right) \tag{22}$$

As is evident from the above expressions, the SMC control law relies on the knowledge of current states, and the rate of change of the reference to compute the control input. For this study, we presumed that full-state feedback, albeit with errors, is available and assumed that the derivative of the reference slip ratio is small.
To calculate the regenerative torque command for the electric motors, we allocate the maximum permissible torque to the motor, and the rest is handled by the friction brakes as and when necessary

$$\tau_{m,i} = \max\left(\tau_{net,i}, \left(g_i \tau_{min,i}\left(\frac{\omega_i}{g_i}, Z\right)\right)\right) \tag{23}$$

where, $\tau_{min,i}$ is the function mapping the motor rotational speed to the maximum possible regenerative torque, at different battery states of charge. This formulation accounts for actuator effort saturation, as governed by the motor torque envelope and the battery charging rate limit while ensuring that maximum energy is recovered during braking instances. Finally, the friction brake command is generated as

$$\tau_{b,i} = \max\left(0, \tau_{net,i} - g_i \tau_{m,i}\right) \tag{24}$$

3 Stability Analysis

The stability of the developed controller is proven by assuming a Lyapunov function, defined as

$$\boldsymbol{V_i} = \frac{1}{2} S_i^2 \tag{25}$$

The derivative of this function is given by

$$\dot{\boldsymbol{V}}_{\boldsymbol{i}} = S_i \times \dot{S}_i \tag{26}$$

Substituting for $\dot{S}_i$ using Eq. (17), we get

$$\dot{\boldsymbol{V}}_{\boldsymbol{i}} = -\frac{\eta S_i}{V} \times \text{sat}\left(\frac{S_i}{\phi_S}\right) \tag{27}$$

From the definition of the saturation function, it follows that

$$\dot{\boldsymbol{V}}_{\boldsymbol{i}} = \begin{cases} \frac{S_i \eta}{V}, & \text{for } S_i \leq -\phi_S \\ -\frac{S_i^2 \eta}{V \phi_S}, & \text{for } -\phi_S < S_i < \phi_S \\ -\frac{S_i \eta}{V} & \text{for } S_i \geq \phi_S \end{cases} \tag{28}$$

As seen, $\dot{\boldsymbol{V}}_{\boldsymbol{i}}$ is negative over the entire domain of S_i. This will guarantee that the sliding surface reaches a boundary layer, of width ϕ_S, within finite time. Note that the traditional SMC formulation uses a signum function, sgn(S), rather than the saturation function, sat$(\frac{S}{\phi_S})$. However, our simulations showed that using the signum function adds undesired chattering to the computed control signals, and thus sat$(\frac{S}{\phi_S})$ was used instead.

4 Results

In this section, we present the results obtained from closed-loop simulation of the developed SMC on the nonlinear coupled vehicle model described by (1)-(11), while adding 5% uncertainty in the form of white noise to the longitudinal wheel slip feedback received by the controller. We test the closed loop system response for an emergency braking scenario, for a section of the US06 cycle, and for starting from an unstable initial condition, i.e., locked wheels. We compare the performance of the developed controller to that of the traditional SMC to demonstrate the superior performance of the proposed formulation. It must be noted that the longitudinal wheel slip ratio and torque values presented in the figures have been normalized with respect to the optimal wheel slip ratio and the maximum motor torque values respectively, to maintain the confidentiality of data.

4.1 Emergency Braking Maneuver

The simulated emergency braking maneuver is a standard 60-0 *mph* braking test to examine and quantify the vehicle's braking capability. We expect our controller to curb the longitudinal wheel slip within the stable region as defined by the Pacejka tire model in (6). This allows us to minimize the braking distance by maximizing the longitudinal tractive force available at the wheels. Fig. (3), (4) and (5) show this braking scenario. Fig. (3) shows the velocity, normalized wheels' slip ratio, and the state and sliding variable dependent parts of the SMC control input for the traditional sliding mode controller, while Fig. (4) shows the corresponding results for the proposed controller in this work. In the bottom sub-plot of Fig. (3), we can see that the sliding mode dependent term, $u^*_{SMC,S}$, of the SMC control input stays constant. For $u^*_{SMC,S}$ to stay constant as the velocity decreases, the sliding variable, S_i itself has to increase, since-

$$u^*_{SMC,S}(t) = \frac{VJ_w}{r_w}\left(\dot{\lambda}_{ref,i} + \eta \times \text{sat}\left(\frac{S}{\phi_S}\right)\right)$$

As the error in wheel slip increases, the state-dependent term for the traditional controller also rapidly diminishes in value. For our proposed controller, however, the sliding surface dependent term is given by Eq. (22), which is independent of the vehicle speed. Hence, the bottom subplot of Fig. (4) shows constant sliding-surface-dependent and state-dependent terms. This allows our developed controller to be able to bring the vehicle to a complete stop faster, while the same is not true for the traditional SMC controller. Further, the bottom subplot of Fig. (3) shows how the traditional SMC controller has significant oscillations in the sliding-surface dependent control input.

The normalized control inputs from the proposed SMC control law and the corresponding normalized motor regenerative torques and friction brake torques are shown in Fig. (5). Since the proposed controller targets the same optimum slip ratio at the front and rear wheels independently, both the front and rear axles are near the maximum longitudinal traction limit. Due to the weight transfer under severe deceleration, we see a large difference in the requested brake torque at the front and rear axles, such that a significantly lower torque is requested on the rear axle. Note that this control maximizes the braking capacity of the vehicle, and it was only possible by accurately accounting for the vehicle weight transfer during braking, without which the rear wheels will be easily locked, resulting in reduced deceleration rate of the vehicle and undermined vehicle safety.

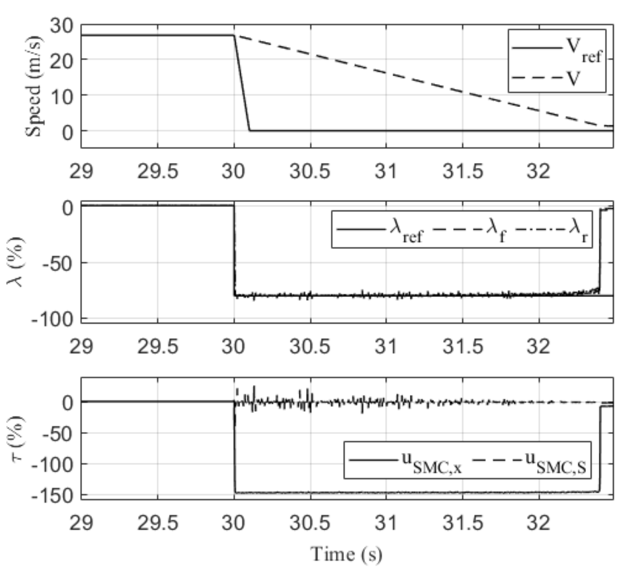

Fig. 3. Vehicle speed (top), normalized longitudinal wheel slip (middle), and SMC control terms (bottom) for traditional SMC for emergency braking maneuver

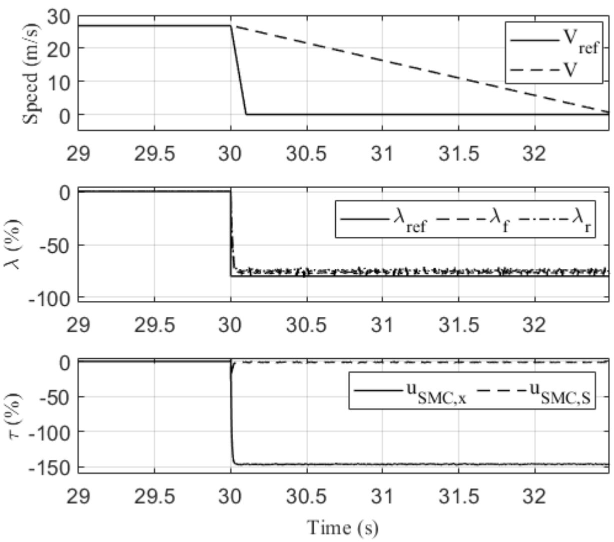

Fig. 4. Vehicle speed (top), normalized longitudinal wheel slip (middle), and SMC control terms (bottom) for emergency braking maneuver using proposed novel SMC controller

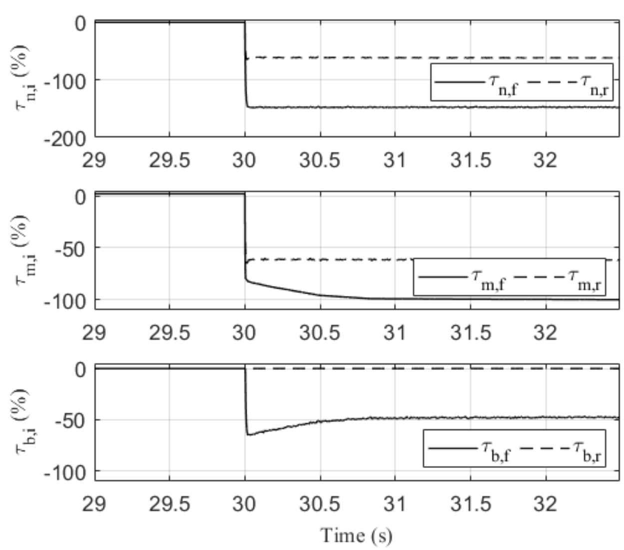

Fig. 5. Normalized net (top), motor (middle), and friction brake (bottom) control torques at the wheel for emergency braking maneuver using proposed SMC controller

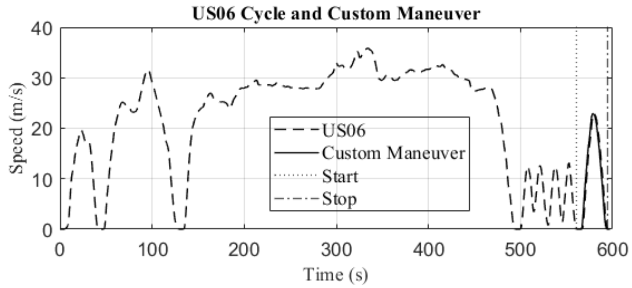

Fig. 6. US06 drive cycle with start and stop times for the simulated maneuver

4.2 US06 Maneuver

To test the proposed controller's performance in another real-world scenario, we simulated the final 35-second leg of the US06 cycle, as shown by the start and stop times in Fig. (6), because it had the sharpest deceleration across the entire cycle. The top plot in Fig. (7) shows the reference and actual vehicle velocity. The middle plot shows the reference and actual wheel slip. Note that the shown reference is the reference input for the SMC and thus it is only non-zero during braking. In the braking section, the controller is unable to achieve perfect reference tracking to compensate for disturbance rejection capability. The bottom plot in Fig. (7) shows sliding surface-dependent, and state-dependent parts of the SMC control inputs. As we can see, the sliding surface-dependent term increases in magnitude when the noise in wheel slip feedback is greatest, right before $t = 30s$.

Fig. (8) shows the commanded normalized motor torques at the wheels. For this scenario, the motors can supply the entire requested braking torque, thus the friction brakes are not activated. This would be true for the rest of the US06 cycle too, at $\zeta = 50\%$, since this particular maneuver has the highest deceleration. As seen, the front and rear motor torques are same in traction, but different under braking. This is because under traction, the torques are split equally, while under braking, we target the same slip ratio on both wheels. This leads to torque commands proportionate to the vertical loads on the respective wheels.

4.3 Stabilization Performance of the Proposed Controller

While applying the regenerative or friction brakes, if the longitudinal wheel slip ratio exceeds the optimal point, the delivered tractive force decreases with increasing absolute wheel slip. In this situation, the wheels eventually stop rotating and lock. One of the primary functions of a good brake controller is to prevent operating in these unstable regions, as it leads to loss of lateral control and increased stopping distance due to saturated tire forces. In the simulations shown above, we targeted the reference slip ratio starting from a stable initial condition. However, in real-world implementation, the wheels might lock for any reason and hence it is important to verify that the developed controller can drive the system to a stable operating region from unstable initial conditions. The top plot of Fig. (9) shows the longitudinal wheel slip response of the front and rear wheels when the simulation starts from an unstable initial condition of $\lambda_i = -1$, which equates to fully locked wheels. As seen, the developed controller can stabilize both the front and rear wheels within less than 0.2 seconds. The front wheels are stabilized slower than the rear ones, since the destabilizing contribution from the state-dependent term of the SMC, shown in the lower plot, is larger due to longitudinal weight transfer, while the sliding surface-dependent term, saturates at the upper threshold dictated by η in Eq. (22).

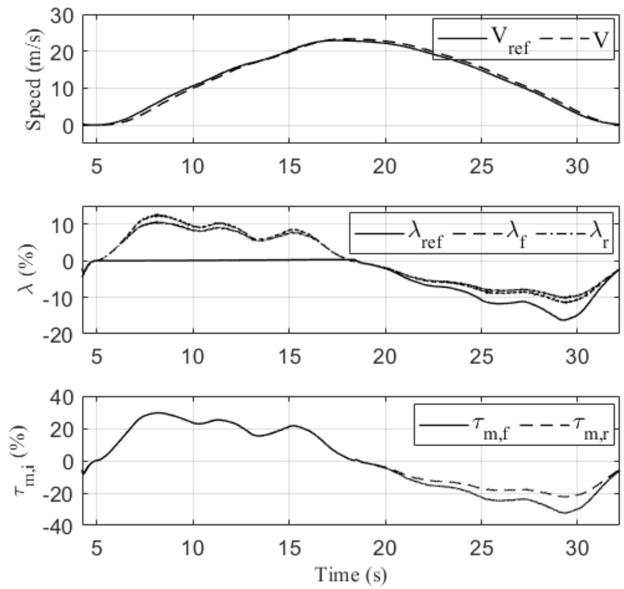

Fig. 7. Vehicle speed (top), normalized longitudinal wheel slip percentage (middle), and SMC control terms (bottom) for custom US06 maneuver

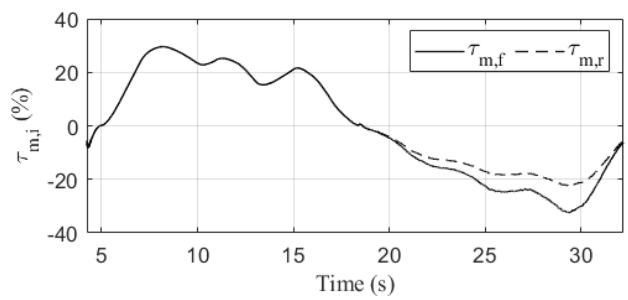

Fig. 8. Normalized motor torques at the wheels for the custom US06 maneuver

5 Conclusion & Future Work

This work proposed a hierarchical control structure for brake control of a dual-motor all-wheel-drive electric vehicle. The control system relies on a novel sliding mode controller that produces total braking torque on the front and rear

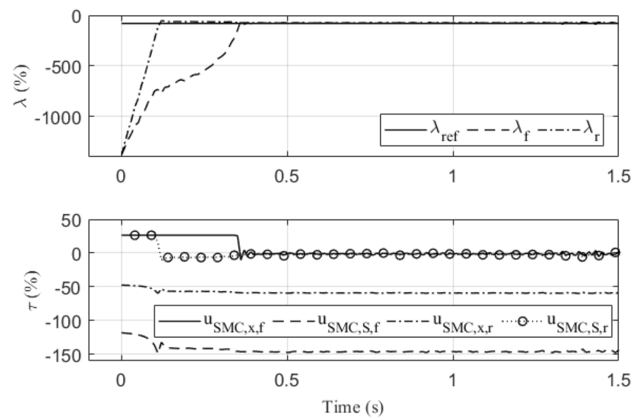

Fig. 9. Normalized longitudinal wheel slip (top) and SMC control torque (bottom) for a braking scenario with unstable initial conditions

axles by accounting for the nonlinear vehicle dynamics and tire model, and the longitudinal weight transfer during braking instances. The torque split controller assigns the maximum permissible braking torque to the electric motors and supplies the rest using the friction brakes. It was shown in the simulations that the proposed controller has better reference tracking and disturbance rejection capabilities over the traditional SMC formulation for an emergency braking scenario. The successful performance of the proposed controller was also demonstrated on a segment of the US06 cycle and for starting from an unstable initial condition.

For this study, we assumed access to erroneous state variables, which, in a real vehicle, need to be calculated from limited and noisy sensor data using state estimators. In the future, the controller will be integrated with an estimator, extended to account for parameter uncertainty, and adapted for deployment on a real-time system. The future research direction could also be to design an improved torque split controller that accurately takes into account the motor, inverter, and battery states and losses. Further, the controller design can be extended to include lateral vehicle dynamics, and account for steering input and spatially varying ground-tire adhesion characteristics.

Acknowledgements

This work was partially funded by support from the U.S. Department of Energy EcoCAR EV Challenge, General Motors Company, and The MathWorks Inc.

References

[1] Kawabe, T., Nakazawa, M., Notsu, I., and Watanabe, Y., 1997. "A sliding mode controller for wheel slip ratio control system". *Vehicle system dynamics,* **27**(5-6), pp. 393–408.

[2] Amodeo, M., Ferrara, A., Terzaghi, R., and Vecchio, C., 2009. "Wheel slip control via second-order sliding-mode generation". *IEEE Transactions on Intelligent Transportation Systems,* **11**(1), pp. 122–131.

[3] Shi, Q., Wang, M., He, Z., Yao, C., Wei, Y., and He, L., 2022. "A fuzzy-based sliding mode control approach for acceleration slip regulation of battery electric vehicle". *Chinese Journal of Mechanical Engineering,* **35**(1), p. 72.

[4] Patra, N., and Datta, K., 2012. "Sliding mode controller for wheel-slip control of anti-lock braking system". In 2012 IEEE International Conference on Advanced Communication Control and Computing Technologies (ICACCCT), IEEE, pp. 385–391.

[5] Filipozzi, L., Assadian, F., Kuang, M., Johri, R., and Alcantar, J. V., 2020. An investigation into the traction and anti-lock braking system control design. Tech. rep., SAE Technical Paper.

[6] Zhu, S., Fan, X., Qi, G., and Wang, P., 2023. "Review of control algorithms of vehicle anti-lock braking system". *Recent Patents on Engineering,* **17**(2), pp. 30–45.

[7] Buckholtz, K. R., 2002. Reference input wheel slip tracking using sliding mode control reference input wheel slip tracking using sliding mode control.

[8] Harifi, A., Aghagolzadeh, A., Alizadeh, G., and Sadeghi, M., 2008. "Designing a sliding mode controller for slip control of antilock brake systems". *Transportation research part C: emerging technologies,* **16**(6), pp. 731–741.

[9] He, L., Ye, W., He, Z., Song, K., and Shi, Q., 2020. "A combining sliding mode control approach for electric motor anti-lock braking system of battery electric vehicle". *Control Engineering Practice,* **102**, p. 104520.